JOURNAL OF APPLIED ELECTROCHEMISTRY 18 (1988) 527–531

Oxygen ion conductivity of the ceria–samarium oxide system with fluorite structure

HIDENORI YAHIRO, YUKARI EGUCHI, KOICHI EGUCHI, HIROMICHI ARAI*

Department of Materials Science and Technology, Graduate School of Engineering Sciences, Kyushu University, 39, Kasugakoen, Kasuga-shi, Fukuoka 816, Japan

Received 16 August 1987; revised 22 November 1987

Ionic conduction of oxygen in the ceria–samarium oxide system was investigated as a function of temperature, partial pressure of oxygen and the oxide composition, together with its crystal structure, density and defect structure. The ionic conductivity of $(CeO_2)_{1-x}(SmO_{1.5})_x$ was the highest in ZrO_2-, ThO_2- and CeO_2-based oxide systems. The system CeO_2–$SmO_{1.5}$ consisted of the solid solution with a fluorite structure at $x < 50$ at. %. The ionic transference number was nearly unity between 600 and 900° C. With an increase in Sm_2O_3 content, the ionic conductivity gradually decreased due to a decrease in mobility of oxygen ions. The samarium oxide-doped ceria was less reducible than pure and alkaline earth oxide-doped ceria.

1. Introduction

There has been much interest in the use of ceria doped with aliovalent cations as a solid electrolyte for oxygen sensors and fuel cells. The other oxide solid electrolytes, doped ZrO_2 [1, 2] and doped ThO_2 [3], are less suitable at low temperatures because of low electrical conductivity and electrode polarization.

Alkaline earth oxides, e.g. CaO [4–6] and SrO [7, 8] and rare earth oxides, e.g. Gd_2O_3 [9, 10] and La_2O_3 [11] have been successfully used as dopants for CeO_2. These dopants are extensively soluble in the ceria sublattice [12]. Substitutions of aliovalent cations for Ce^{4+} result in the formation of oxygen vacancy sites to compensate the charge balance in the lattice. Thus, the solid solution becomes predominantly ionic conductive for oxygen over an extended temperature and oxygen pressure range.

Of the alkaline earth elements, Ca and Sr have been studied as dopants for CeO_2 in a previous study [5, 8]. The electrical conductivities of CaO- and SrO-doped ceria are much higher than that of stabilized zirconia. The composition range with high value of electrical conductivity was very large for ceria-based solid electrolytes [13].

Ceria–rare earth oxide systems are characterized by their large solubility limit and their electrical properties have been partly reported [14, 15]. However, the electrochemical properties of the most ionic conductive ceria-based oxides, e.g. the system CeO_2–Sm_2O_3, have not been fully reported as a function of additive content. In the present work, the electrical conductivity and ionic transference number of the CeO_2–rare earth oxide systems, in particular the CeO_2–$SmO_{1.5}$ system, were investigated. The crystal structure, density and defect structure are discussed.

2. Experimental details

2.1. *Sample preparation*

Polycrystalline powder was prepared from ceria and rare earth oxides. The mechanically mixed powder with the calculated amount of CeO_2 (99.9% pure) and Sm_2O_3 (99.9% pure) or rare earth oxide was calcined at 1300° C for 10 h, then pulverized and pressed isostatically into a disk (20 mm in diameter and 3 mm thickness) at 2.7 t cm^{-3} *in vacuo*. The disk was sintered at 1650° C for 15 h. A sample with the same composition was also prepared from cerium and samarium nitrates (98.0% and 99.9% pure, respectively). The metal nitrates were dissolved in water and heated at 80–90° C. Ammonia water (28% molarity) was added to the solution until the metals completely precipitated as hydroxides. After heating at 500° C for 1 h the powder was calcined at 1300° C for 10 h. Then, the sintered disk was obtained by the above-mentioned procedure.

The crystal structure was determined by X-ray diffraction using CuK_α radiation. Crystalline MgO powder was added as an internal standard for diffraction angles. The density of the sintered sample was measured by a water pycnometric technique.

2.2. *Measurement of ionic transference number*

An oxygen concentration cell of the type

$$P_{O_2},\ Pt/(CeO_2)_{1-x}(SmO_{1.5})_x/Pt,\ P'_{O_2} \qquad (1)$$

was used to obtain the ionic transference number of samples as a function of temperature. The theoretical e.m.f. of this cell is given by

$$E_{theor} = (RT/4F)\ln(P'_{O_2}/P_{O_2}) \qquad (2)$$

* Author to whom correspondence should be addressed.

0021-891X/88 $03.00 + .12

where R is the universal gas constant, T the absolute temperature and F Faraday's constant. The ionic transference number is given by

$$t_i = E_{meas}/E_{theor} \quad (3)$$

where E_{meas} is the observed open circuit e.m.f. for the cell. In the present measurements, P_{O_2} was fixed at 1 atm and the e.m.f. was obtained as a function of P'_{O_2} (1.0×10^{-3}–0.21 atm). The electromotive force of a gas concentration cell was measured over the temperature range 600–900° C with a gas flow rate of 200–300 $cm^3 min^{-1}$. On each flat cylindrical disk surface, a platinum paste (Tanaka Matthey, KT-5) was applied as an electrode and fired at 1000° C for 10 min to obtain an electrical contact. The disk was attached to a mullite tube by fusion welding of silver to ensure gas tightness of the cell at elevated temperatures.

2.3. *Measurement of electrical conductivity*

The electrical conductivity of a sintered sample (15 mm × 4 mm × 5 mm) was measured as a function of temperature and oxygen partial pressure by a conventional d.c. four probe method. The region of higher oxygen pressure ($P_{O_2} = 10^{-5}$–1 atm) was obtained with O_2–N_2 mixtures while that of lower oxygen pressure ($P_{O_2} < 10^{-10}$ atm) was obtained with CO–CO_2 mixtures. Electrical contacts between current probes and the sample were made by platinum wires and paste. A galvanostatic d.c. source was used to supply current to these probes. Potential probes were located between two current probes by tightly winding platinum wires around the sample. The potential drop between two potential probes was measured using a digital voltmeter.

2.4. *Gravimetric analysis of the samples*

The reducibility of the ceria–samarium oxide system was measured as a function of oxygen partial pressure by an electrically controlled balance (Shimadzu Co., TGA-41). The oxygen partial pressure was controlled by use of a CO–CO_2 gas mixture. The weight loss of samples with oxygen removal was monitored as a function of P_{O_2}.

3. Results and discussion

3.1. *The structure and electrical conductivity of rare earth oxide-added ceria*

The mixing of a small amount of rare earth oxide with ceria leads to the quantitative formation of oxygen vacancies because of charge compensation. The crystal structure and electrical conductivity of a series of ceria–rare earth oxides were measured. The rare earth-doped ceria samples were hereafter denoted as $(CeO_2)_{1-x}(MO_{1.5})_x$. The crystal structure of pure CeO_2 is the cubic fluorite type. The diffraction patterns of the rare earth oxide-doped ceria $x < 0.1$ are essentially unchanged from that of pure CeO_2 except for slight shifts in diffraction angles. These shifts are due to dissolution of the additives in the fluorite lattice. The lattice constant obtained from the diffraction angles was dependent on the ionic radius of the ionic additives to ceria, as shown in Fig. 1. The addition of ions with larger radius than Ce^{4+} ($r = 0.097$ nm) leads to an increase in the lattice constant in the fluorite structure, while the addition of small ions reduces the lattice constant. Figure 1 shows the lattice constants of ceria with 20 at. % of added rare earth oxides. The lattice constant increases linearly with the ionic radius of the additive cation. This relation supports the formation of a solid solution between ceria and rare earth oxides. The rare earth oxides were more soluble in the ceria lattice than were the alkaline earth oxides [5]. Some of the systems are completely soluble in the fluorite lattice.

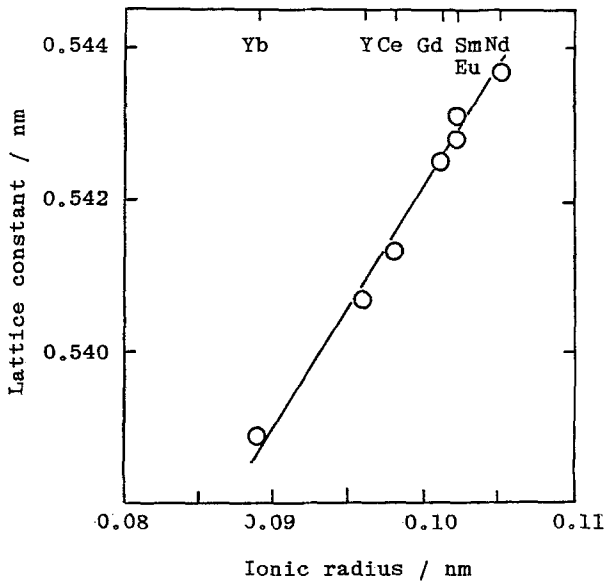

Fig. 1. The relationship between lattice constant and radius of dopant cation for $(CeO_2)_{0.80}(MO_{1.5})_{0.20}$ in fluorite structure.

The ionic transference number, t_i, and the electrical conductivity of the CeO_2–rare earth oxide systems were measured by an oxygen concentration cell and a d.c.-4 probe method, respectively. The values of electrical conductivity and ionic transference number at

Table 1. Ionic conductivities and ionic transference numbers of ceria–rare earth oxide systems at 800° C

Sample	$\sigma_i \times 10^2$ ($S\,cm^{-1}$)	t_i
$(CeO_2)_{0.80}(SmO_{1.5})_{0.20}$	9.45	1.00
$(CeO_2)_{0.80}(DyO_{1.5})_{0.20}$	7.74	0.98
$(CeO_2)_{0.80}(HoO_{1.5})_{0.20}$	6.39	1.00
$(CeO_2)_{0.80}(NdO_{1.5})_{0.20}$	5.93	1.00
$(CeO_2)_{0.80}(ErO_{1.5})_{0.20}$	5.74	0.97
$(CeO_2)_{0.80}(YbO_{1.5})_{0.20}$	5.59	1.00
$(CeO_2)_{0.80}(TmO_{1.5})_{0.20}$	5.59	1.00
$(CeO_2)_{0.80}(GdO_{1.5})_{0.20}$	5.53	0.99
$(CeO_2)_{0.80}(LaO_{1.5})_{0.20}$	4.16	1.00
$(CeO_2)_{0.80}(CaO)_{0.20}$	4.28	0.99
CeO_2	0.03	0.35
$(ZrO_2)_{0.92}(Y_2O_3)_{0.08}$	3.01	1.00

800° C are summarized in Table 1. The addition of rare earth oxides to ceria sharply enhanced the ionic transference number due to the formation of oxygen vacancies. The values were almost unity for every rare earth oxide–ceria system. The electrical conductivity was also enhanced by the addition of rare earth oxide. In particular, the ionic conductivity of $(CeO_2)_{0.80}(SmO_{1.5})_{0.20}$ was 1.5–2.0 times higher than that of $(CeO_2)_{0.80}(GdO_{1.5})_{0.20}$ reported previously [9, 15] or shown in Table 1. The ceria–samarium oxide system exhibited the highest electrical conductivity among the ceria-based oxides. The electrical properties of ceria–samarium oxide systems will be further examined in detail.

3.2. *The structure and density of* $(CeO_2)_{1-x}(SmO_{1.5})_x$

The X-ray diffraction patterns of $(CeO_2)_{1-x}(SmO_{1.5})_x$ systems consisted of the lines from the fluorite-type structure of CeO_2, but the lines from undissolved $SmO_{1.5}$ were not observed up to $x = 0.6$. The dissolution of the $SmO_{1.5}$ in the fluorite lattice is obvious from the increase in lattice constant. The lattice constant of CeO_2–$SmO_{1.5}$ systems increased sharply at $x < 0.3$, but it was maximum and almost constant at $x > 0.4$ (Fig. 2). The lattice expansion corresponds to the larger ionic radius of Sm^{3+} (0.109 nm) than that of Ce^{4+} (0.097 nm). Although precipitation of the second phase cannot be observed at $0.4 < x < 0.6$ from X-ray diffraction patterns, the constant lattice constant in this region implies the ordering of samarium ions in a fluorite lattice. Therefore, the solubility limit of samarium in a fluorite lattice is $0.4 < x < 0.6$, which is larger than that of alkaline earth oxide–ceria systems. In the crystal structure of rare earth oxides, there are four types of structure, i.e. A-, B-, C- and fluorite-oxide structure. The crystal structures of samarium oxide and ceria are C-type rare earth oxide and fluorite-type, respectively. The structures resemble each other. Not only the structural similarity, but also the similar ionic size between Ce^{4+} and Sm^{3+} contribute to the large solubility limit. On the other hand, the alkaline earth oxides possess a rock-salt-like structure. The structure of ceria–rare earth oxide systems appears to be better stabilized than that of ceria–alkaline earth oxide systems.

The density of sintered $(CeO_2)_{1-x}(SmO_{1.5})_x$ oxides is shown in Fig. 2. The dotted line in this figure indicates the theoretical density calculated from the unit cell dimension and the average molecular weight of the sample. In this calculation, a homogeneous solid solution of $SmO_{1.5}$ and CeO_2 is assumed at $0 < x < 0.5$. The measured density of the CeO_2–$SmO_{1.5}$ system agrees with the theoretical at every composition within experimental error. The samples used in the present study have above 95% of the theoretical density.

3.3. *Electrical properties of* $(CeO_2)_{1-x}(SmO_{1.5})_x$

The ionic transference numbers of the CeO_2–$SmO_{1.5}$ system obtained from e.m.f. measurement are shown in Fig. 3. Although the ionic transference number of undoped ceria is only 0.3–0.4, those of the CeO_2–$SmO_{1.5}$ system were greatly enhanced. The CeO_2–$SmO_{1.5}$ samples were regarded as almost pure ionic conductors over a wide composition range ($0 < x < 0.4$) at 600–900° C. However, in the composition range of $x > 0.5$ the ionic transference number of samples decreased slightly. The contribution of p-type conduction is sometimes observed for oxide ionic conduction at high partial pressure of oxygen. The p-type conduction is promoted by doping with a cation of lower valency in the host lattice. The decrease in t_i at high concentration of $SmO_{1.5}$ is explained by the appearance of p-type electrical conductivity indicated from electrical conductivity measurement as a function of oxygen partial pressure.

The ionic conductivity is defined as the product of the ionic transference number and electrical conduc-

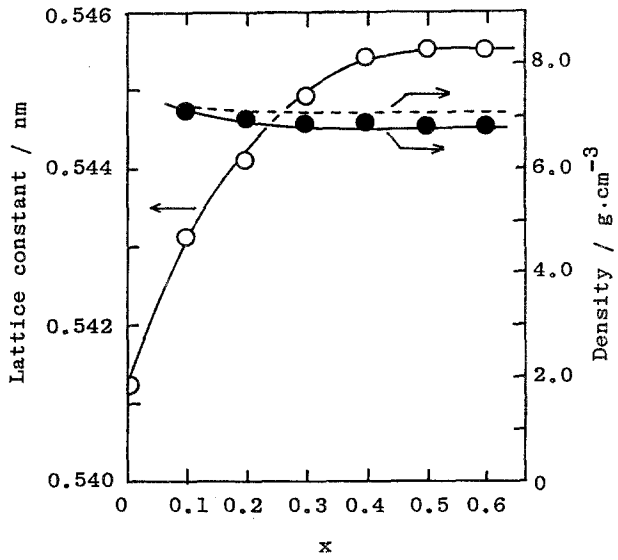

Fig. 2. Composition dependence of lattice constant and density for $(CeO_2)_{1-x}(SmO_{1.5})_x$. ○, Lattice constant; ●, observed density; -----, theoretical density.

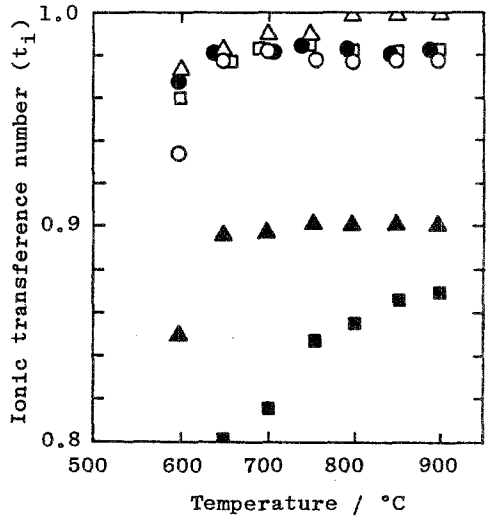

Fig. 3. Temperature dependence of ionic transference numbers for $(CeO_2)_{1-x}(SmO_{1.5})_x$. ○, $x = 0.1$; △, $x = 0.2$; □, $x = 0.3$; ●, $x = 0.4$; ▲, $x = 0.5$; ■, $x = 0.6$.

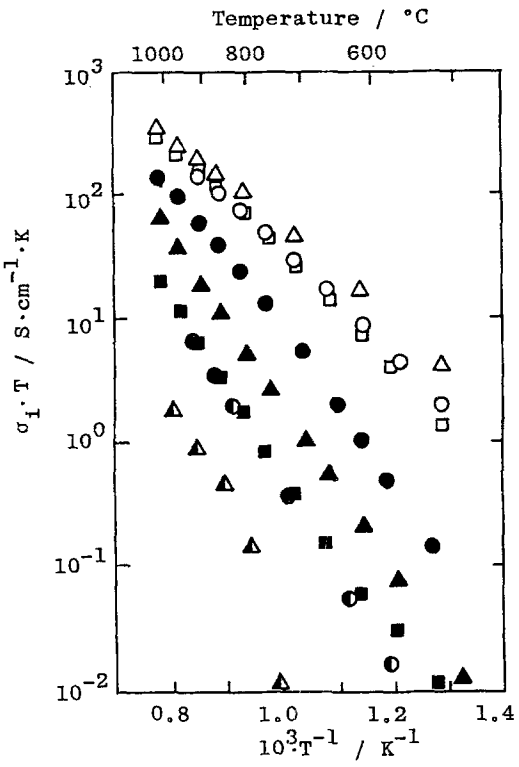

Fig. 4. Arrhenius plots of the ionic conductivities of $(CeO_2)_{1-x}(SmO_{1.5})_x$ in air. (○) $x = 0.1$; (△) $x = 0.2$; (□) $x = 0.3$; (●) $x = 0.4$; (▲) $x = 0.5$; (■) $x = 0.6$; (◭) CeO_2; (◐) $(ZrO_2)_{0.85}(CaO)_{0.15}$.

tivity. Arrhenius plots of the ionic conductivity in air are shown in Fig. 4. The addition of a small amount of $SmO_{1.5}$ significantly enhances the ionic conductivity of samples because of the formation of a large number of oxygen vacancies, $V_O^{\cdot\cdot}$, in the fluorite lattice, as expressed by the following reaction.

$$2SmO_{1.5} \xrightarrow{CeO_2} 2Sm'_{Ce} + O_O + V_O^{\cdot\cdot} \qquad (4)$$

The ionic conductivity of $(CeO_2)_{0.80}(SmO_{1.5})_{0.20}$ is 2 orders of magnitude higher than that of pure ceria in the temperature range 800–1000° C. The slope of the Arrhenius plot gives the apparent activation energy for transfer of the oxygen ion.

$$\sigma_i T = A \exp(-E_a/kT) \qquad (5)$$

The activation energy for $(CeO_2)_{1-x}(SmO_{1.5})_x$ ($0 < x < 0.3$) was much smaller than those for calcia-stabilized zirconia and pure ceria. The activation energy for $(CeO_2)_{0.80}(SmO_{1.5})_{0.20}$ was 0.78 eV, being the lowest in the family of ceria-based oxides. The electrical conductivity of the ceria–samarium oxide system is plotted as a function of samarium oxide content in Fig. 5. The ionic conductivity of $(CeO_2)_{1-x}(SmO_{1.5})_x$ increased sharply at $x < 0.1$, and was maximum at $x = 0.2$. The decrease in ionic conductivity at $x > 0.3$ was gradual, as compared with that reported for stabilized zirconia [17]. The number of oxygen vacancies increases with increasing $SmO_{1.5}$ content within its solubility limit to maintain charge neutrality; however, the ionic conductivity decreased even within the solubility limit. This implies a decrease in the mobility of vacancies at the high dopant concentration. The

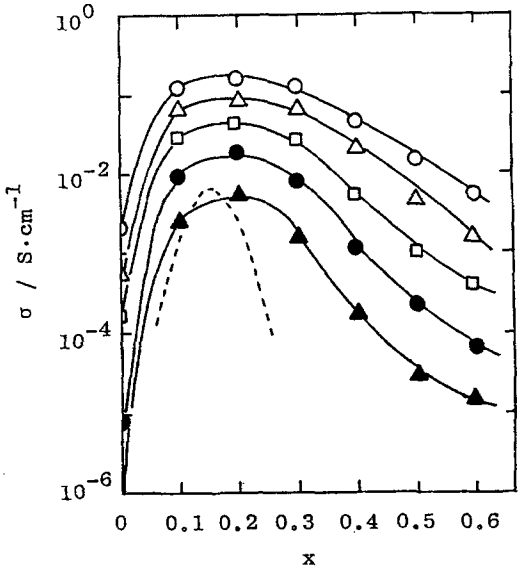

Fig. 5. Composition dependence of conductivities for $(CeO_2)_{1-x}(SmO_{1.5})_x$. (○) 900° C; (△) 800° C; (□) 700° C; (●) 600° C; (▲) 500° C; (– – – –) $(ZrO_2)_{1-x}(CaO)_x$ at 800° C.

crystal structure of C-type rare earths is regarded to be a fluorite-type structure with ordered oxygen vacancies. Partial ordering or pair formation of vacancies appears to occur even within the solubility limit but is not so large as to be observed as a phase separation. The decrease in ionic conductivity is attributed to the ordering of oxygen vacancies [16].

The electrical conductivity of $(CeO_2)_{1-x}(SmO_{1.5})_x$ and $(CeO_2)_{0.80}(CaO)_{0.20}$ was measured as a function of oxygen partial pressure, as shown in Fig. 6. Under high oxygen partial pressure, the ionic conduction was operative, as can be judged from the constant electrical conductivity. Under low oxygen partial pressure, however, the electrical conductivity increased. This increase is attributed to the appearance of n-type electronic conduction due to the reduction of ceria. The number of free electrons increased accompanied by removal of oxygen in the fluorite lattice. The elec-

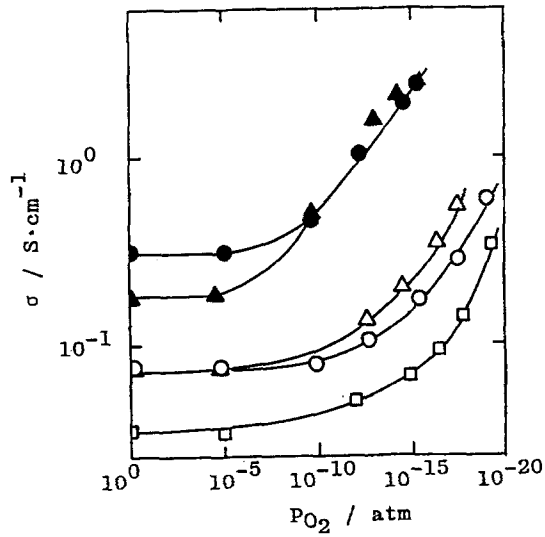

Fig. 6. Electrical conductivities as a function of oxygen partial pressure for $(CeO_2)_{1-x}(SmO_{1.5})_x$. △, $x = 0.1$ (800° C); ○, $x = 0.2$ (800° C); □, $x = 0.3$ (800° C); ●, $x = 0.2$ (1000° C); ▲, $(CeO_2)_{0.80}(CaO)_{0.20}$ (1000° C).

trical conductivity in the n-type region decreased with an increase in the oxygen vacancy concentration with the $SmO_{1.5}$ content compared with the concentration of free electrons.

The ionic conductivity of $(CeO_2)_{0.80}(SmO_{1.5})_{0.20}$ was compared with the previous result for $(CeO_2)_{0.80}(CaO)_{0.20}$ at 1000° C. Ionic and n-type conduction mechanisms were also clearly observed for the ceria–calcia system. The transition to the n-type region occurs at $P_{O_2} = 10^{-5}$ atm for $(CeO_2)_{0.80}(CaO)_{0.20}$, but at $P_{O_2} = 10^{-7}$ atm for $(CeO_2)_{0.80}(SmO_{1.5})_{0.20}$. A wide ionic conduction range is desirable for application of ceria-based oxides as solid electrolytes. The X-ray diffraction measurements indicated that the solubility limit of CaO in CeO_2 is 23 mol %. Thus, both $(CeO_2)_{0.80}(SmO_{1.5})_{0.20}$ and $(CeO_2)_{0.80}(CaO)_{0.20}$ consist of homogeneous solid solutions. The concentration of oxygen vacancies introduced by the charge compensation of dopants is expected to be nearly twice as large for Ca^{2+} addition than for Sm^{3+} addition due to the difference in cation valency. The higher ionic conductivity of $(CeO_2)_{0.80}(SmO_{1.5})_{0.20}$, however, indicates that the mobility of oxygen vacancies is higher than in $(CeO_2)_{0.80}(CaO)_{0.20}$.

As for the electronic conduction at low P_{O_2}, doping with cations of lower valency is known to suppress the n-type conduction. Doping with Sm^{3+} is expected to bring about higher electronic conduction than doping with Ca^{2+}. However, the conductivity of $(CeO_2)_{0.80}(SmO_{1.5})_{0.20}$ coincided with $(CeO_2)_{0.80}(CaO)_{0.20}$ at $P_{O_2} = 10^{-10}$ atm (1000° C). As described below, the suppression of electronic conduction in $(CeO_2)_{0.80}(SmO_{1.5})_{0.20}$ is due to its resistance to reduction. The reducibility of the solid solution was evaluated from gravimetric changes of samples accompanied by the removal of oxygen at low oxygen partial pressure (Fig. 7). The weight loss of the sample was expressed as a deviation from the stoichiometry, δ, in $(CeO_{2-\delta})_{1-x}(MO_n)_x$ where $MO_n = SmO_{1.5}$ or CaO. The weight loss of $(CeO_2)_{0.80}(CaO)_{0.20}$ agreed with that of undoped CeO_2, however, that of $(CeO_2)_{0.80}(SmO_{1.5})_{0.20}$ was obviously smaller. The samarium oxide-doped ceria was less reducible than calcia-doped ceria. This result suggested that the reducibility of the solid solution was dependent on the different cations added to the ceria.

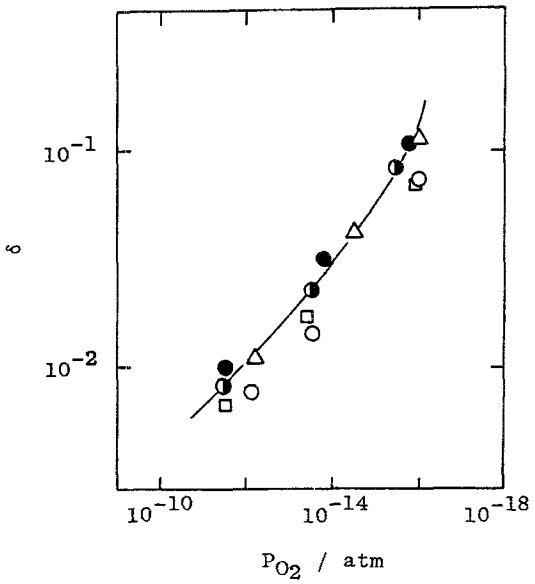

Fig. 7. Isothermal plot of weight loss with the deviation from nonstoichiometry, δ, vs P_{O_2} for $(CeO_{2-\delta})_{1-x}(MO_n)_x$ at 1000° C. △, $(CeO_2)_{0.90}(SmO_{1.5})_{0.10}$; ○, $(CeO_2)_{0.80}(SmO_{1.5})_{0.20}$; □, $(CeO_2)_{0.70}(SmO_{1.5})_{0.30}$; ●, $(CeO_2)_{0.80}(CaO)_{0.20}$; ◑, CeO_2.

4. Conclusion

The cation-doped ceria showed excellent ionic conductivity and high ionic transference number. The ionic conductivity of $(CeO_2)_{0.80}(SmO_{1.5})_{0.20}$ was 1.5–2.0 times higher than that of $(CeO_2)_{0.80}(GdO_{1.5})_{0.20}$ and the highest in the family of cation-doped ceria. The system CeO_2–Sm_2O_3 maintained high ionic conductivity over a wide composition range due to its high solubility limit. It is evident that the samarium oxide-doped ceria was less reducible than alkaline earth oxide systems or undoped ceria. The excellent ionic conductivity, as well as the resistance to reduction of samarium oxide-doped ceria, indicates the usefulness of this material as an oxide electrolyte material for, for example, third generation fuel cells.

References

[1] A. Nakamura and J. B. Wagner Jr, *J. Electrochem. Soc.* **127** (1980) 2325.
[2] M. J. Verkerk, B. J. Middelhuis and A. J. Burggraaf, *Solid State Ionics* **6** (1982) 159.
[3] W. L. Worrell, *Topics in Applied Physics* **21** (1977) 143.
[4] R. N. Blumenthal and B. A. Pinz, *J. Appl. Phys.* **38** (1976) 2376.
[5] H. Arai, T. Kunisaki, Y. Shimizu and T. Seiyama, *Solid State Ionics* **20** (1986) 241.
[6] K. Eguchi, T. Kunisaki and H. Arai, *Comm. Am. Ceram. Soc.* **69** (1986) 282.
[7] R. N. Blumenthal and J. E. Garnier, *J. Solid State Chem.* **16** (1976) 21.
[8] H. Yahiro, K. Eguchi and H. Arai, *Solid State Ionics* **21** (1986) 37.
[9] T. Kudo and H. Obayashi, *J. Electrochem. Soc.* **122** (1975) 142.
[10] I. Riess, D. Braunshtein and D. S. Tannhauser, *J. Am. Ceram. Soc.* **64** (1981) 479.
[11] T. Takahashi and H. Iwahara, *Denki Kagaku* **34** (1966) 254.
[12] T. H. Etsell and S. N. Flengas, *Chem. Rev.* **70** (1970) 339.
[13] H. Arai, K. Eguchi and H. Yahiro, 'Proc. 2nd IMCS' (1986) p. 335.
[14] G. Brauer and H. Gradinger, *Z. Anorg. Allg. Chem.* **276** (1954) 209.
[15] R. T. Distine, R. N. Blumenthal and T. F. Kuech, *J. Electrochem. Soc.* **126** (1979) 264.
[16] E. C. Subbarao and H. S. Maiti, *Solid State Ionics* **5** (1981) 539.
[17] T. Kudo, in 'Rare Earths, Properties and Applications' (edited by T. Kano and H. Yanagida), Gihodo, Tokyo (1980) p. 267.